

**MECHANISM RESEARCH ON THE DISPROPORTIONATION FOR PREPARING
DICHLORODIMETHYLSILANE CATALYZED BY $(\text{AlCl}_2)^+$ MODIFIED 4T
 $\text{NaAlCl}_4/\text{ZSM-5}$**

Wen-Yuan Xu^{1*}, Xiao-Dan Qin¹, Shao-Ming Yang¹, Zan-Ru Guo¹, Zhi-Li Fang¹ and San-Guo Hong²

¹School of Material Science and Engineering, East China Jiaotong University, Nanchang 330013, China

²College of Chemistry, Nanchang University, Nanchang 330031, China

(Received September 28, 2018; Revised April 10, 2019; Accepted April 20, 2019)

ABSTRACT. Disproportionation for preparing $(\text{CH}_3)_2\text{SiCl}_2$ can effectively solve some problems caused by the accumulation of by-products during direct synthesis. In this paper, the disproportionation for preparing $(\text{CH}_3)_2\text{SiCl}_2$ catalyzed by $(\text{AlCl}_2)^+$ modified 4T $\text{NaAlCl}_4/\text{ZSM-5}$ was studied, and the reaction mechanism was investigated under B3LYP/6-311G++(3df, 2pd) basis using density functional theory. It was found that the activation energies of the rate determining step in the main reaction and side reaction were 97.89 $\text{kJ}\cdot\text{mol}^{-1}$ and 169.50 $\text{kJ}\cdot\text{mol}^{-1}$, respectively. Moreover, the skeleton stability of 4T cluster $\text{NaAlCl}_4/(\text{AlCl}_2)^+-\text{ZSM-5}$ was higher and its activity was better than $(\text{AlCl}_2)^+$ modified before due to its lower Mayer bond order and slightly larger four-center bond order. Our results from activation energy analysis, vibration analysis, IRC calculation, LOL analysis and bond order analysis showed good consistency with each other and agreed well with those of previous experiments.

KEY WORDS: $\text{AlCl}_3/\text{ZSM-5}$, Disproportionation, DFT, $(\text{CH}_3)_2\text{SiCl}_2$

INTRODUCTION

Organic silicon materials [1-3] are a kind of high-performance materials of silicon. They are mainly inorganic structure chains with organic groups as side chain, and possess the advantages of both inorganic and organic compounds [4]. For the preparation of organic silicon materials, the top priority is to synthesize high-quality monomer $(\text{CH}_3)_2\text{SiCl}_2$ [5, 6] (M2). However, owing to the necessity of boosting the M2 market, the direct synthesis method [7, 8] produces a growing number of by-products, i.e., CH_3SiCl_3 (M1) and $(\text{CH}_3)_3\text{SiCl}$ (M3), which accumulate during the synthesis process and cause various problems. In view of this, more attention has been paid to the disproportionation reaction [9-11] for producing M2 using M1 and M3 as reactants. Fan Hong *et al.* [12] used amines and metal chlorides as catalysts to produce M2 through the disproportionation reaction, and the content of M2 in the final product reached 46.4%. Further, they pointed out that $\text{AlCl}_3/\text{Al}_2\text{O}_3$ had better activity with Lewis acid as active site and achieved an M2 yield of 60.6%. In addition, Zhang Ning [13] used MCM-type mesoporous amine as catalyst to produce M2 through the similar reaction, and the content of M2 was 38.3%.

Studies showed that ZSM-5 zeolite [14, 15] and NaAlCl_4 [16] both had catalytic effects on the disproportionation reaction. In previous experiments [17, 18], the catalytic activities of the 3T, 4T, 5T and 6T cluster ZSM-5 zeolite and the Mg, Al modified 5T cluster ZSM-5 molecular sieve were studied, and the 4T cluster ZSM-5 zeolite showed good catalytic effects in the disproportionation for preparing M2. In order to further study the catalytic effects of ZSM-5 and NaAlCl_4 , in this paper, the catalytic activities of Al-modified 4T cluster $\text{NaAlCl}_4/(\text{AlCl}_2)^+-\text{ZSM-5}$ (Cat.II) were theoretically calculated, and the results were compared with 4T cluster $\text{NaAlCl}_4/\text{ZSM-5}$ (Cat.I) [17] of our previous experimental results.

*Corresponding author. xwyktz@163.com

This work is licensed under the Creative Commons Attribution 4.0 International License

CALCULATION METHOD

The structures of reactants, intermediates and products were investigated under B3LYP/6-311G++(3df, 2pd) basis using density functional theory (DFT) [19] in the disproportionation reaction catalyzed by Cat.I or Cat.II. In order to ensure the calculation accuracy, the structures of transition states and the reaction pathways were identified through vibration analysis and calculated through intrinsic reaction curves (IRC) [20]. Then the energies were corrected by the secondary perturbation MP2/6-311++G(3df,2pd) method. Finally, the zero point energy (ZPE) [21] correction was also considered.

RESULTS AND DISCUSSION

Previous experiments [22] showed that NaAlCl_4 was firstly reduced to AlCl_3 in the reaction and finally returned to double salt. In order to illustrate the mechanism of their disproportionation in one figure, both Cat.I and Cat.II were endowed with the same active sites (Figure 1). As Figure 1 shows, Lewis acid active sites $-\text{AlCl}_2$ appear during the disproportionation reaction catalyzed by Cat.I or Cat.II. As the reaction was going on, bonds Na^1-Cl^2 and Na^1-Cl^3 break. The bond length of Na^1 and Cl^1 gradually shortens to 2.4110 nm from 0.2659 nm and finally generate NaCl [22]. Hence, subsequent discussion directly uses the structure of $\text{AlCl}_3/\text{ZSM-5}$. The calculated eigen values of reactants and products are positive, and the transition states have only one negative eigen value, which proves that the transition states are correct. The minor frequencies caused by fixed bonds are small enough to be negligible.

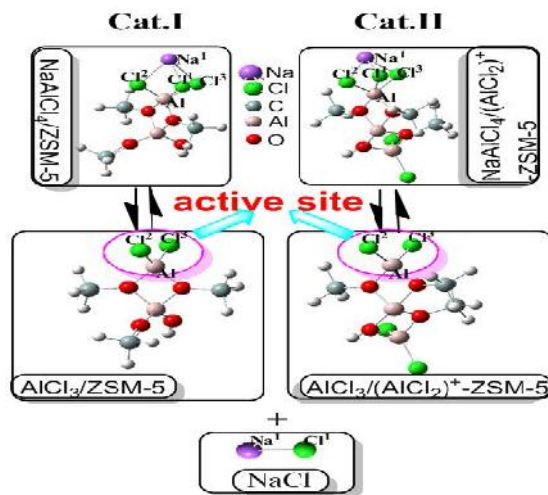


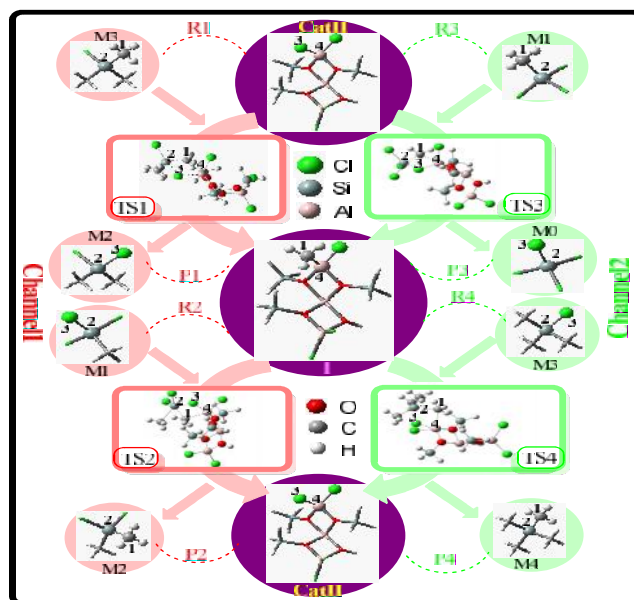
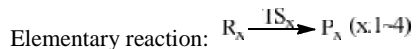
Figure 1. Structures of Cat.I and Cat.II and their active sites.

There are similar reaction mechanism and transition states for Cat.I and Cat.II in the catalytic disproportionation to produce M2. In the case of Cat.II, as shown in Figure 2, the disproportionation reaction proceeds in two main channels. (M3 and Cat.II are called R1, M2 and I are called P1, and so on).

Channel 1 (the main reaction): M3 reacts with Cat.II firstly, and then generates intermediate I and M2 through the transition state TS1. Next, M1 reacts with I through TS2, and produces Cat.II and M2.

Table 1. Bond distance of the key atoms of each structure in the reaction process (nm).

Cat.I	R1	TS1	P1	R2	TS2	P2
$\text{C}^1\text{-Si}^2$	0.1906	0.4315	0.5159	0.4676	0.2870	0.1885
$\text{Si}^2\text{-Cl}^3$	0.4531	0.2384	0.2216	0.2156	0.2352	0.4350
$\text{Cl}^3\text{-Al}^4$	0.2192	0.3599	0.5459	0.4484	0.2423	0.2206
$\text{Al}^4\text{-C}^1$	0.4571	0.2203	0.1961	0.1959	0.2180	0.4869
	R3	TS3	P3	R4	TS4	P4
$\text{C}^1\text{-Si}^2$	0.1874	0.2306	0.4780	0.5337	0.2917	0.1904
$\text{Si}^2\text{-Cl}^3$	0.4325	0.2238	0.2127	0.2230	0.2424	0.5711
$\text{Cl}^3\text{-Al}^4$	0.2201	0.3661	0.4470	0.5638	0.2191	0.1908
$\text{Al}^4\text{-C}^1$	0.3704	0.2073	0.1961	0.1960	0.2165	0.5533
Cat.II	R1	TS1	P1	R2	TS2	P2
$\text{C}^1\text{-Si}^2$	0.2206	0.3255	0.4709	0.4104	0.1887	0.1886
$\text{Si}^2\text{-Cl}^3$	0.5851	0.3628	0.2058	0.2157	0.3805	0.4621
$\text{Cl}^3\text{-Al}^4$	0.1853	0.2152	0.3154	0.3908	0.2197	0.2120
$\text{Al}^4\text{-C}^1$	0.4261	0.2772	0.2061	0.1968	0.5158	0.6999
	R3	TS3	P3	R4	TS4	P4
$\text{C}^1\text{-Si}^2$	0.1875	0.4659	0.4689	0.7337	0.1920	0.1917
$\text{Si}^2\text{-Cl}^3$	0.3848	0.3642	0.2253	0.2230	0.4962	0.5868
$\text{Cl}^3\text{-Al}^4$	0.2207	0.2232	0.3905	0.7638	0.2193	0.2191
$\text{Al}^4\text{-C}^1$	0.5209	0.1955	0.1960	0.1960	0.5216	0.5591

Figure 2. Reaction process of the 4T cluster $\text{AlCl}_3/(\text{AlCl}_2)^+$ -ZSM-5 catalyst.

M0: SiCl_4 ; M1: CH_3SiCl_3 ; M2: $(\text{CH}_3)_2\text{SiCl}_2$; M3: $(\text{CH}_3)_3\text{SiCl}$; M4: $\text{Si}(\text{CH}_3)_4$; I: Intermediate.

Channel 2 (the side reaction): M1 reacts with Cat.II firstly, and then generates intermediate I and SiCl_4 through the transition state TS3. Next, M3 reacts with I through TS4, and produces Cat.II and $\text{Si}(\text{CH}_3)_4$. Table 1 shows the bond distance of key atoms of each structure in Channel 1 and Channel 2, respectively. To identify the structure of each transition state, vibration analysis of fully optimized transition structure was carried out in this study, and the results are illustrated in Figure 3. Imaginary frequency of the transition state is derived from the stretching vibration of Al^4 , Cl^3 , Si^2 and C^1 atoms. Taking TS1 as an example, as C^1 and Al^4 atoms come close to each other, then Cl^3 - Al^4 bond is broken and Al^4 - C^1 bond is formed. At the same time, for M3, as Si^2 and Cl^3 atoms come close to each other, then C^1 - Si^2 bond and Cl^3 - Al^4 bond are broken, and Cl^3 - Si^2 bond and C^1 - Al^4 bond are formed, thus generating product P1. On the other hand, C^1 - Si^2 bond and Cl^3 - Al^4 bond are formed to generate reactant R1. TS1 has the tendency of moving towards R1 and P1 synchronously. It is further proved that the identification of TS1 is accurate and reliable. The atomic trends of TS2 ~ TS4 are similar to that of TS1, as shown in Figure 3. From Figures 2 and 3, it can be concluded that the key of the reaction is the departure of Cl^3 atom on the active site Al^4 - Cl^3 , which enables Al^4 to accept the electron pair of $-\text{CH}_3$ or $-\text{Cl}$ on silane. This is the characteristic of Lewis acid and agrees well with the experimental conclusions of Fan Hong *et al.* [12].

Figure 4 shows the spacing trends of key atoms along the IRC pathways catalyzed by Cat.I and Cat.II. During the whole process from transition states to final products, the key atomic spacing shows a gradually lengthening or shortening tendency, which confirms the transition states and the correct connection of reactants and products. This result is matched with Figure 3 and Figure 2, indicating that the reaction mechanism and vibration mode of the transition states are believable.

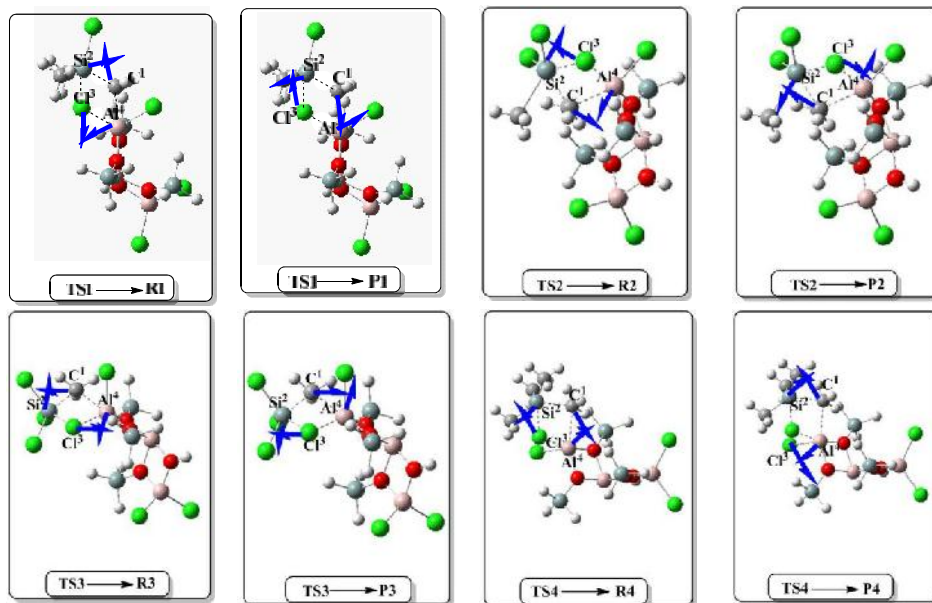


Figure 3. Vibration modes of the transition states in the case of Cat.II.

Based on the density functional theory (DFT) and the energy gradient method, the energies of all stationary points in the potential energy surface are optimized, and the zero-point energies (ZPEs) are corrected using basis set of MP2/6-311++G(3df,2pd). Figure 5 shows the activation

energies and reaction heats of each step. In the main reaction, the activation energies of the rate determining step catalyzed by Cat.I and Cat.II are $100.26 \text{ kJ}\cdot\text{mol}^{-1}$ and $97.89 \text{ kJ}\cdot\text{mol}^{-1}$, respectively. In the side reaction, the activation energies of the rate determining step are $279.47 \text{ kJ}\cdot\text{mol}^{-1}$ and $169.50 \text{ kJ}\cdot\text{mol}^{-1}$, respectively. The activation energies of the rate determining step in main reaction are lower than those in side reaction, which proves that the reaction of preparing M2 is the main reaction. These results are consistent with our earlier experimental results [22].

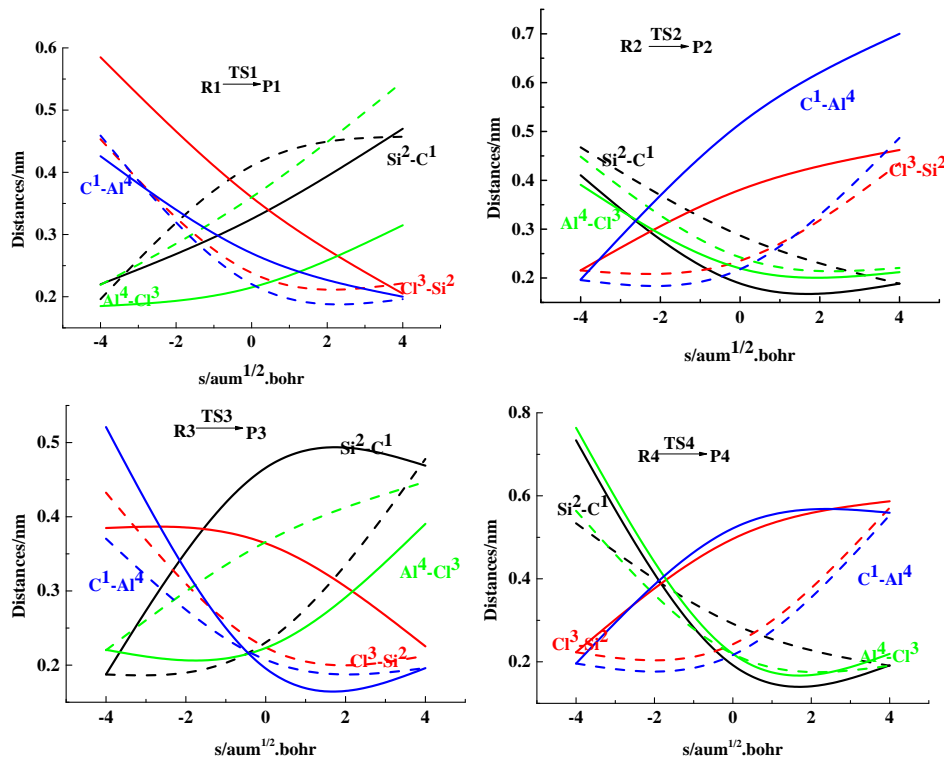


Figure 4. Spacing trends of key atoms along the IRC pathways in the system (---Cat.I, —Cat.II).

By comparing the activation energies of the rate determining step in the main reaction, it can be seen that the activation energy of Cat.II is slightly lower than that of Cat.I, indicating that the catalytic effect of Cat.II is better than that of Cat.I. The purpose of modification is to increase the load of NaAlCl_4 . As can be seen from the structure of Figure 1, the modified sites are similar to existing active site, and can provide new active site of Al-Cl. These results are consistent with previous experimental results [23]. Compared with Cat.I catalyst system, the introduction of $(\text{AlCl}_2)^+$ makes the reaction easier to proceed, that is, the catalytic effect of Cat.II is better.

In order to further explore the activation effect of catalyst and more intuitively understand the localized electrons, these two catalysts were analyzed with LOL Analysis. The catalytic systems of Cat.I and Cat.II were optimized, and Mayer bond order of Al-Cl and four-center bond order of Al^4 , Cl^3 , O^1 and O^2 were calculated. Figure 6 shows the LOL Analysis results of Cat.I and Cat.II.

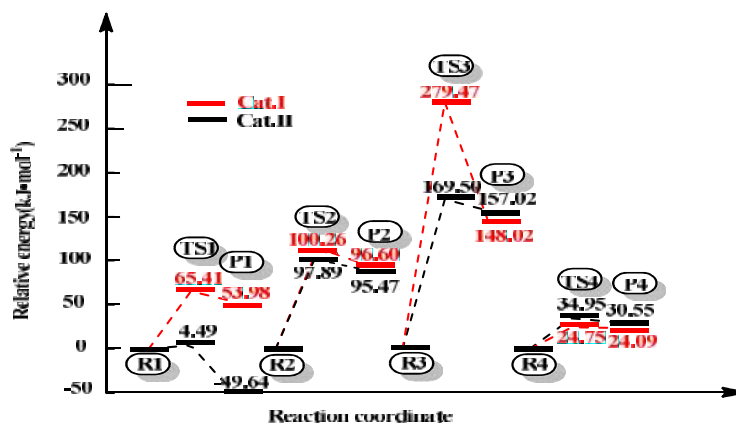


Figure 5. Activation energies and reaction heats of Cat.I and Cat.II.

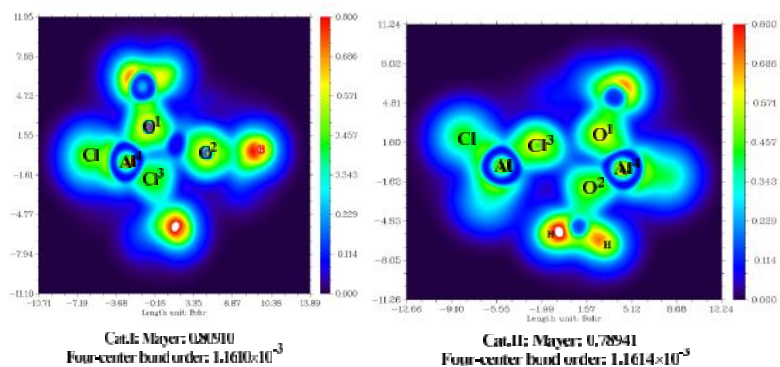


Figure 6. LOL analysis results of Cat.I and Cat.II.

Compared with Cat.I, Mayer bond order in Cat.II is lower, indicating that Al-Cl bond is easier to break; but the four-center bond order is slightly larger, indicating that the molecular skeleton of Al⁴, Cl³, O¹ and O² is more stable. Hence, the activity and stability of Cat.II are higher than those of Cat.I. Both indicate that electron delocalization ability of Cat.I is relatively weaker than that of Cat.II, and Al-Cl bond of Cat.II is easy to break. Compared with Al⁴ atom of Cat.I and Cat.II, central electron of Al in Cat.I has stronger localization, but Al in Cat.II has stronger delocalization, which indicates that Al in Cat.II is more active. And the surrounding electrons of both Al⁴ can be delocalized, but that delocalization ability in Cat.II is stronger than that in Cat.I. At the same time, the same conclusion is gained when all skeleton O atoms in Cat.I and Cat.II are discussed. The electron of skeleton O (Cat.II) can more easily delocalize active site Cl, which can promote CH₃ of silanes to attack active site Cl, so the disproportionation can be proceeded more easily. This not only proves that the activity of Cat.II is better, but also proves that the active site provider of Al-Cl is Lewis acid [12].

According to Figure 6, Cat.II has higher skeleton stability and better activity than Cat.I. This accords well with the analysis result of their activation energies. From the Al (modified

site) on the right side of Cat.II, it can be seen that the electron delocalization capability of Al-Cl is similar to that of the active site on the left side and can be predicted as a new active site.

This is in good accordance with the structure of Figure 1 and preliminary experiments [10]. The catalytic effect of Cat.II is better than Cat.I, because the introduction of $(\text{AlCl}_2)^+$ changes the electron cloud density of acidic sites ($-\text{AlCl}_2$) of 4T cluster $\text{NaAlCl}_4/\text{ZSM-5}$ and makes the reaction easier. Therefore, the Cl atom on the active site Al-Cl of Cat.II is more likely to leave, which makes it easier for the Al atom to accept $-\text{CH}_3$ or $-\text{Cl}$ of the reaction system. As a result, the disproportionation reaction is easier to occur, that is, Cat.II has better activity than Cat.I. This matches well with the results of vibration analysis and IRC calculation.

CONCLUSIONS

In summary, the disproportionation reaction for preparing $(\text{CH}_3)_2\text{SiCl}_2$ catalyzed by $(\text{AlCl}_2)^+$ modified 4T $\text{NaAlCl}_4/\text{ZSM-5}$ was investigated, and the reaction mechanism was analyzed under B3LYP/6-311G++(3df, 2pd) basis using density functional theory. Some conclusions can be drawn as follows: (1) Activation energies of the rate determining step in the main reaction and side reaction were $97.89 \text{ kJ}\cdot\text{mol}^{-1}$ and $169.50 \text{ kJ}\cdot\text{mol}^{-1}$, respectively. (2) Mayer bond orders of Cat.I and Cat.II are 0.80910 and 0.78941 respectively, and their four-center bond orders are 1.1610×10^{-3} and 1.1614×10^{-3} , respectively. (3) Cat.II has better stability and activity than Cat.I, and its active site Al-Cl shows the characteristic of Lewis acid in the reaction. (4) The results from activation energy analysis, vibration analysis, IRC calculation, LOL Analysis and bond order analysis showed good consistency with each other and agreed well with those of previous experiments.

ACKNOWLEDGEMENTS

This study was supported by the National Natural Science Foundation of China (No. 21563011, No. 21872049, and No. 21465012).

REFERENCES

1. Martin, C.J.; Philip, H.Z. Local inhibition of angiogenesis by halofuginone coated silicone materials. *J. Mater. Sci.: Mater. Med.* **2012**, *23*, 1203-1210.
2. Iva, S.; Tanabe, A.; Maeda, T.; Funamizu, H.; Aizu, Y. Development of non-deterioration-type skin tissue phantom using silicone material. *Opt. Rev.* **2014**, *21*, 353-358.
3. Wang, D.X.; Zuo, Y.J.; Liu, H.; Feng, L.L.; Li, A.H.; Feng, S.Y. Focus on research of international organosilicon chemistry. *Silicone Mater.* **2015**, *29*, 125-138.
4. Gordon, A.D.; Hinch, B.J.; Strongin, D.R. Effects of individual promoters on the direct synthesis of methylchlorosilanes. *J. Catal.* **2009**, *266*, 291-298.
5. Xu, W.Y.; He, Z.Y.; Chen, Y.; Li, F.Y.; Hong, S.G. Research on the disproportionation of DFT and MP2 for preparing dichlorodimethylsilane catalyzed by $\text{AlCl}_3(\text{II})$. *Acta Chim. Sinica* **2005**, *63*, 1474-1478.
6. Pakizeh, M.; Moghadam, A.N.; Omidkhah, M.R.; Namvar, M.M. Preparation and characterization of dimethyldichlorosilane modified SiO_2/PSf nanocomposite membrane. *Korean J. Chem. Eng.* **2013**, *30*, 751-760.
7. Ivanov, A.V.; Graham, G.W.; Shelef, M. Adsorption of hydrocarbons by ZSM-5 zeolites with different $\text{SiO}_2/\text{Al}_2\text{O}_3$ ratios: A combined FTIR and gravimetric study. *Appl. Catal. B* **1999**, *21*, 243-258.

8. Fang, H.R.; Huang, K.K.; Yuan, L.; Wu, X.F.; Wang, D.; Chen, H.W.; Feng, S.H. The direct synthesis of Au nanocrystals in microdroplets using the spray-assisted method. *New J. Chem.* **2016**, *40*, 7294-7298.
9. Eiichi, S.; Youichi, N.; Masaki, O.; Yoshio, O. Disproportionation of triethoxysilane over $\text{KF}/\text{Al}_2\text{O}_3$ and heat-treated hydrotalcite. *Appl. Catal. A* **1998**, *167*, 7-10.
10. Cai, D.L. Study on catalytic disproportionation of silicone low boiling of aluminum trichloride. *Silicone Mater.* **2017**, *31*, 183-186.
11. Grote, F.; Gruber, C.; Börrnert, F.; Kaiser, U.; Eigler, S. Thermal disproportionation of oxo-functionalized grapheme. *Angew. Chem. Int. Ed.* **2017**, *56*, 9222-9225.
12. Wang, X.F.; Tan, J.; Fan, H.; Bu, Z.Y.; Li, B.G. Application of supported AlCl_3 catalyst in preparation of dimethyldichlorosilane by redistribution method. *Chem. Eng.* **2006**, *34*, 66-69.
13. Tan, Y.P.; Zhang, N.; Wang, J.H.; Yao, L. Synthesis, characterization and activity of a new mesoporous catalyst for cracking of organosilane high boiling residues. *J. Chem. Ind. Eng.* **2008**, *59*, 2800-2803.
14. Parisa, D.; Vithaya, R. Theoretical investigation of ethanol conversion to ethylene over H-ZSM-5 and transition metals-exchanged ZSM-5. *Catal. Lett.* **2012**, *142*, 143-149.
15. Yue, Y.Y.; Kang, Y.; Bai, Y.; Gu, L.L.; Liu, H.Y.; Bao, J.; Wang, T.H.; Yuan, P.; Zhu, H.B.; Bai, Z.S.; Bao, X.J. Seed-assisted, template-free synthesis of ZSM-5 zeolite from natural aluminosilicate minerals. *Appl. Clay Sci.* **2018**, *158*, 177-185.
16. Yin, D.H.; Li, C.Z.; Tao, L.; Yu, N.Y.; Hu, S.; Yin, D.L. Synthesis of diphenylmethane derivatives in Lewis acidic ionic liquids. *J. Mol. Catal. A-Chem.* **2006**, *245*, 260-265.
17. Xu, W.Y.; Yang, M.; Liu, Y.X.; Guo, Z.R.; Hu, L.; Yang, S.M.; Hong, S.G. Disproportionation mechanism of methylchlorosilane catalyzed by different clusters $\text{AlCl}_3/\text{ZSM-5}$. *J. Chem. Sci.* **2018**, *130*, 58-64.
18. Xu, W.Y.; Yao, C.J.; Xu, Y.C.; Hong, S.G. Theoretical study for disproportionation of dimethyldichlorosilane catalyzed by $\text{NaAlCl}_4/\text{X-ZSM-5}$. *Asian J. Chem.* **2017**, *29*, 104-108.
19. Shityakov, S.; Roewer, N.; Förster, C.; Broscheit, J.A. In silico modeling of indigo and tyrian purple single-electron nano-transistors using density functional theory approach. *Nanoscale Res. Lett.* **2017**, *12*, 439-446.
20. Bao, Y.F.; Liu, Z.Z.; Liu, D.S.; Ge, X.W. Theoretical study on the structural and optoelectronic properties of the linear perfluorooctane sulfonate (PFOS). *Chinese J. Struct. Chem.* **2013**, *32*, 1348-1356.
21. Zhao, G.Z. Theoretical study on intermolecular interactions of 4-amino-3,5-dinitropyrazole dimers. *J. At. Mol. Phys.* **2017**, *34*, 1-8.
22. Xu, W.Y.; Wan, H.H.; Wang, L.W.; Hong, S.G. Theoretical calculation for disproportionation of methyltrichlorosilane and trimethylchlorosilane catalyzed by $\text{NaAlCl}_4/\text{ZSM-5}$. *Asian J. Chem.* **2016**, *28*, 1624-1628.
23. Xu, W.Y.; Hao, W.; Zhong, Y.; He, Z.Y.; Liu, J.P.; Zheng, L.Z.; Hu, L. Modification of $\text{NaAlCl}_4/\text{ZSM-5}$ zeolite catalyst—effect on the disproportionation reaction of organosilicon monomer and trimethyl. *Zhejiang Univ. (Sci. Ed.)* **2010**, *37*, 72-75.